Discovery and Characterization of a Novel Dihydroisoxazole Class of α-Amino-3-hydroxy-5-methyl-4-isoxazolepropionic acid (AMPA) Receptor Potentiators

ARTICLE *in* JOURNAL OF MEDICINAL CHEMISTRY · NOVEMBER 2013

Impact Factor: 5.45 · DOI: 10.1021/jm401274b · Source: PubMed

Journal of Medicinal Chemistry

Article

pubs.acs.org/jmc

Discovery and Characterization of a Novel Dihydroisoxazole Class of α-Amino-3-hydroxy-5-methyl-4-isoxazolepropionic acid (AMPA) Receptor Potentiators

Nandini C. Patel,[†] Jacob Schwarz,[‡] Xinjun J. Hou,[†] Dennis J. Hoover, Longfei Xie, Anton J. Fliri, Randall J. Gallaschun, John T. Lazzaro, Dianne K. Bryce,[§] William E. Hoffmann, Ashley N. Hanks,[†] Dina McGinnis,[∥] Eric S. Marr, Justin L. Gazard, Mihály Hajós,[⊥] Renato J. Scialis, Raymond S. Hurst,[#] Christopher L. Shaffer,[†] Jayvardhan Pandit,* and Christopher J. O'Donnell*

Pfizer Worldwide Research and Development, Groton Laboratories, 445 Eastern Point Road, Groton, Connecticut 06340, United States

Supporting Information

ABSTRACT: Positive allosteric modulators ("potentiators") of α-amino-3-hydroxy-5-methyl-4-isoxazolepropionic acid (AMPA) receptors (AMPAR) enhance excitatory neurotransmission and may improve the cognitive deficits associated with various neurological disorders. The dihydroisoxazole (DHI) series of AMPAR potentiators described herein originated from the identification of **7** by a high-throughput functional activity screen using mouse embryonic stem (mES) cell-derived neuronal precursors. Subsequent structure-based drug design using X-ray crystal structures of the ligand-binding domain of human GluA2 led to the discovery of both PF-04725379 (**11**), which in tritiated form became a novel ligand for characterizing the binding affinities of subsequent AMPAR potentiators in rat brain homogenate, and PF-04701475 (**8a**), a prototype used to explore AMPAR-mediated pharmacology in vivo. Lead series optimization provided **16a**, a functionally potent compound lacking the potentially bioactivatable aniline within **8a**, but retaining desirable in vitro ADME properties.

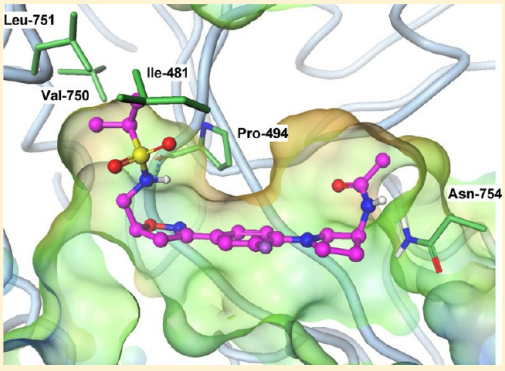

INTRODUCTION

Glutamate, which mediates the majority of excitatory neurotransmission in the mammalian brain, is released from presynaptic terminals to activate a variety of glutamatergic receptors on a diverse population of neurons and glia. Ionotropic glutamate receptors comprise three postsynaptic subtypes differentiated by their unique responses to the selective agonists α-amino-3-hydroxy-5-methyl-4-isoxazolepropionic acid (AMPA), *N*-methyl-D-aspartate (NMDA), and kainate.[1] Activated AMPA receptors (AMPARs) depolarize neuronal membranes leading to increased NMDA receptor-mediated Ca^{2+}-gating[2] that affects synaptic morphology and function[3] believed to underlie learning and memory.[4] Thus, AMPAR activation has been proposed to ease the cognitive deficits of diseases such as schizophrenia and Alzheimer's disease.[5]

Unlike orthosteric agonists, AMPAR positive allosteric modulators ("potentiators") lack intrinsic activity. However, in the presence of glutamate, they augment agonism by modulating the biophysical properties of the receptor. It has been demonstrated that AMPAR potentiators binding at different allosteric sites can attenuate either receptor deactivation (increasing synaptic current amplitude) or both receptor deactivation and desensitization (increasing and prolonging synaptic current). Consistent with AMPAR potentiators having these effects on synaptic currents, they have been shown to reduce the threshold and elevate the ceiling of long-term potentiation, increase the task-specific firing activity of hippocampal neurons, and enhance stimulation-induced hippocampal theta-oscillation; all of which have been proposed to represent a pro-cognitive profile.[3b,5] These observations are supported by the nootropic effects of AMPAR potentiators in both animal models[6] and in some but not all small clinical trials.[7] In addition to cognitive enhancement, AMPAR potentiators have shown activity in other neurodisease animal models of anxiety, attention-deficit hyperactivity disorder, Parkinson's disease, and depression.[6b,8]

AMPARs have four subunits organized as a dimer of dimers.[9] For each subunit, its extracellular portion contains an amino-terminal domain (ATD) and a ligand-binding domain (LBD), while its transmembrane portion comprises three alpha helices (TM1, TM3, and TM4) and a re-entrant hairpin loop (TM2) on the intracellular side of the membrane. The intracellular C-terminus of the receptor has been shown to possess interaction sites for a variety of proteins involved in receptor trafficking and

Received: August 16, 2013
Published: November 11, 2013

dx.doi.org/10.1021/jm401274b | J. Med. Chem. 2013, 56, 9180−9191

synaptic plasticity. There are four subtypes of AMPAR subunits (GluA1−4) that are functionally organized as hetero- or homotetramers; additional structural diversity is conferred by RNA editing and alternative RNA splicing generating flip (i) and flop (o) variants for each subunit.[10] The flip/flop cassette, in a sequence-dependent manner, regulates the rate of channel closing and desensitization.[11]

There are many solved cocrystal structures of the AMPAR LBD with bound potentiators.[12] The membrane-proximal LBD has a bilobate structure, which has been shown to adopt open and closed conformations depending on whether it is bound to antagonists or agonists, respectively.[12,13] Glutamate binding to the LBD triggers lobe closure to initiate the gating cascade. AMPAR potentiators bind at the LBD dimer interface and preferentially stabilize the LBD in its active (closed) conformation. Different modes of allosteric activation are possible as indicated by experiments demonstrating that potentiators can differentially affect receptor deactivation and desensitization to enhance receptor signaling.[14]

A diverse array of chemotypes (Figure 1), distinguished by their receptor interactions, have been reported to potentiate

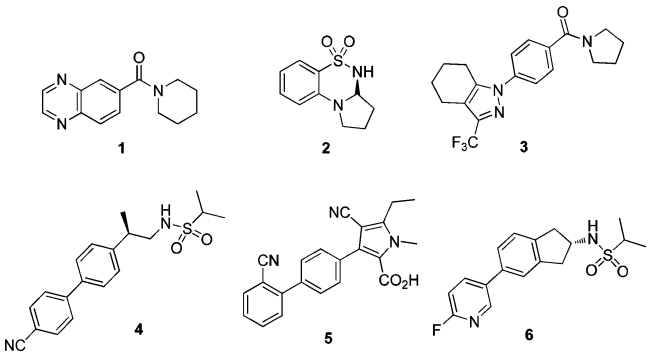

Figure 1. Representative structures of AMPAR potentiator chemotypes.

AMPARs.[15] One group of compounds, characterized by the benzamides (represented by **1**, CX516),[16] the benzothiadiazines (**2**, S18986),[17] and the trifluomethyltetrahydroindazole carboxamides (**3**, GSK732973),[18] attenuates receptor deactivation with minimal to modest effects on receptor desensitization. Another group, exemplified by the phenethylsulfonamides (**4**, LY451646),[19] the heterocyclic carboxylic acids (**5**, LY2059346),[20] and the amino indane sulfonamides (**6**, GSK729327),[21] has a primary affect of impeding receptor desensitization.

Considering the structural diversity and multiple binding modes of allosteric AMPAR potentiators, opportunities remain to identify and explore new molecules to expand the knowledgebase of this pharmacological class. The highlighted molecules (Figure 1) were reportedly discovered by using homotetrameric AMPAR functional assays to elucidate structure−activity relationships (SAR) and, for the phenethylsulfonamides, to identify a radioligand for in vitro AMPAR binding assays.[22] However, because of the AMPAR complexities emphasized previously and because it is unclear which subunit combination(s) affords an optimal therapeutic agent, we used a functional assay employing mouse embryonic stem (mES) cell-derived neurons to profile compounds against a native constellation of AMPAR subtypes and their associated proteins to generate amalgamated pharmacologic values.[23] The assay was specifically configured for the identification of AMPAR potentiators. In this article, we disclose a new molecular class of potentiators identified in a high-throughput screen (HTS) of the Pfizer compound file utilizing this assay. Specifically, we discuss the medicinal chemistry strategy, guided by X-ray crystal structures of the AMPAR LBD-bound HTS lead followed by iterative structure-based drug design (SBDD) with the careful consideration of physicochemical properties that confer favorable absorption, distribution, metabolism, and excretion (ADME) characteristics, which identified both a novel radioligand to establish a proprietary AMPAR potentiator binding assay and a novel prototype to explore the in vivo pharmacology of this class. The developed binding assay and the in vivo characterization of the prototype compound are also disclosed.

RESULTS AND DISCUSSION

Discovery of a Novel AMPAR Radioligand. An HTS of the Pfizer screening library using a fluorometric imaging plate reader (FLIPR)-based mES cell-derived neuronal precursors functional assay[23] identified DHI (*S*)-**7** (EC_{50} of 4.4 μM) as an AMPAR potentiator, which was originally prepared during the identification of novel structural motifs to replace the oxolidinone of the linezolid structural class (Figure 2).[24] With a molecular weight (MW) of 305 amu, calculated logP (clogP) of 2.0, topological polar surface area (TPSA) of 54 Å^2, **7** seemed a favorable starting point for molecular optimization considering the physicochemical properties associated with orally administered small molecule drugs targeting the central nervous system (CNS).[25] From an in vitro ADME perspective,[26] **7** had good permeability (P_{app} of 35 × 10^{-6} cm/s), no P-glycoprotein (P-gp) liability (MDR1-transfected MDCK Efflux Ratio (ER) of 0.98), and modest human liver microsome-projected clearance ($CL_{int,app}$ = 26 μL/min/mg). Accordingly, the goal of SAR studies initiating from **7** was to improve functional potency while maintaining optimal CNS-centric physicochemical and ADME properties.

Crystal structures of the AMPAR LBD show a binding site for potentiators at the interface between two subunits of the LBD.[27] The binding site straddles a crystallographic 2-fold axis of symmetry, which relates two subunits of the LBD, and can accommodate either two ligands bound symmetrically (e.g., cyclothiazide[27b]) or a single ligand bound asymmetrically that is able to bind in two different orientations with equal affinity. A 1.5 Å resolution X-ray cocrystal structure with **4** was determined internally at the time of the HTS campaign, and this structural information was incorporated into the hit optimization strategy. Initially, the cocrystal structure of the GluA2o LBD and **4** was used as a computational docking model for the binding of **7**. Since **7** is chiral and at the time of its discovery it was unknown which enantiomer would be preferred by the receptor, each enantiomer was individually modeled using an internal proprietary docking program[28] to understand its interaction with the LBD. Through multi-sampling docking simulation it was determined that the original *S*-enantiomer identified from the HTS aligned well with **4** (Figure 2) and provided the best fit in the binding pocket. The acetamide of **7** occupied the hydrophobic pocket formed by Ile-481, Leu-751, and Val-750, with its amide hydrogen forming a hydrogen bond with the backbone carbonyl of Pro-494. In this docking model, the pyrrolidine of **7** overlays with the nitrile of **4** and approaches Asn-754. For confirmation, the X-ray structure of **7** bound to the glutamate-bound LBD of human

dx.doi.org/10.1021/jm401274b | J. Med. Chem. 2013, 56, 9180−9191

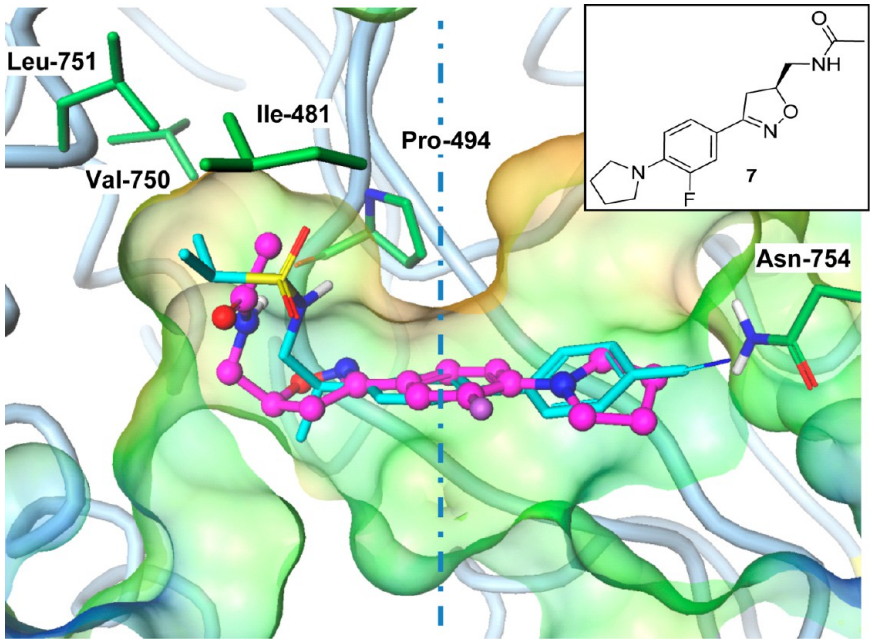

Figure 2. X-ray cocrystal structure of **7** (magenta) superimposed on the X-ray structure of **4** (cyan) in the symmetrical binding pocket of the human GluA2o LBD. Only one binding pose for each compound is shown for clarity. Analogous to the sulfonamide hydrogen of **4**, the amide hydrogen of **7** forms a hydrogen bond with the backbone carbonyl oxygen of Pro-494.

GluA2o was determined at 2.1 Å resolution (Figure 2), and it clearly showed **7** occupying the allosteric site at the dimer interface of two LBD subunits. As with **4**, **7** binds equally in two symmetrical orientations. Its acetamide projects into one deep pocket, similar to the sulfonamide in **4**.

This structure immediately suggested design ideas to improve the potency of **7**. First, it was hypothesized that replacing the acetamide with a sulfonamide would better fill the hydrophobic pocket to produce a more functionally potent compound while maintaining desirable drug-like properties. The initial replacement of the acetamide of **7** with the isopropyl sulfonamide of **4** to give **8** afforded a 100-fold improvement in activity as a racemate. Following enantiopurification of **8**, functional analysis showed its *S*-enantiomer (PF-04701475, **8a**), which had acceptable physicochemical and in vitro ADME properties, to be most potent (Table 1). Attempts to expand the SAR of the acetamide region of **7** through small amide and sulfonamide libraries, along with exploring its replacement with simple carbamates and ureas, was largely unfruitful. Notably, functional activity was lost (i.e., EC_{50} > 32 μM) upon such substitutions but retained by low molecular weight sulfonamide or amide moieties.

Modeling **8a** into the crystal structure of **7** bound to AMPAR suggested its pyrrolidine was making important interactions within the binding pocket, and this was confirmed as pyrrolidine-lacking **9** was inactive (EC_{50} > 32 μM). Des-fluoro analogue **10** was slightly less potent than **8**, indicating that the aryl fluorine might regulate only a minor interaction with the binding pocket as supported by the cocrystal structure. Furthermore, it appeared that the second hydrophobic pocket within the binding site could be accessed through pyrrolidine substitution, which might confer greater functional potency. This speculation was explored by placing an acetamide at the 3-position of the pyrrolidine to afford **11**, and it was confirmed by both the high functional potency of **11** (EC_{50} < 10 nM, Table 1) and its X-ray cocrystal structure (Figure 3) that the acetamide advantageously reached into the second (symmetry-related) binding pocket.

Because of its high potency in functional activity in the mES assay, a tritiated form of **11** [^{3}H]PF-04725379, with a specific activity of 44.2 Ci/mmol, was prepared to develop an AMPAR potentiator binding assay using cell membrane preparation from rat cortical tissues and modifying described methodology.[29] Since it is reported that glutamate enhances the binding of an AMPAR potentiator radioligand, saturations were performed with L-glutamate (500 μM).[29] Saturation binding studies determined a K_D of 4.8 nM (n = 2) and B_{max} of 22,220 CPM (n = 2) of **11** in rat cortical tissue. Subsequently, a competition binding assay was developed with **11**, and the K_i values derived from it helped further validate the enantiospecific functional activity of **8a** and **8b** and additional analogues (Table 1).

Optimization of the DHI Series to Improve ADME Properties. The design of **11** demonstrated that the structure-based design strategy of making a ligand that simultaneously occupies both LBD hydrophobic pockets can indeed lead to a highly potent AMPAR potentiator. However, its high MW (427 amu) and TPSA (109 Å^2) resulted in poor permeablility (P_{app} of 3.9 × 10^{-6} cm/s) and high P-gp liability (MDR1 ER of 12.1). As suggested by these in vitro ADME parameters, **11** was not brain penetrant in mice (brain-to-plasma compound concentration ratio (C_b:C_p) of 0.03) hindering its use to characterize the AMPAR-mediated pharmacology of this DHI class in vivo.

Consequently, the SAR around **8a** was revisited, where replacements for its aniline moiety were first sought to derisk the well-documented concerns of idiosyncratic drug reactions associated with aniline-containing molecules.[30] The crystal structures of **4**, **7**, and **11** indicated that substituting the pyrrolidine with an aromatic ring could be accommodated within the AMPAR LBD. Accordingly, pyrrolidine replacement with a phenyl group (**12** vs **8**, Table 1) significantly decreased functional potency; however, replacing it with a 3-pyridyl group

dx.doi.org/10.1021/jm401274b | J. Med. Chem. 2013, 56, 9180−9191

Table 1. ADME Properties

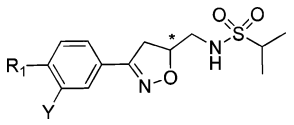

Entry	*	R_1	Y	EC_{50} (nM)[a]	Emax (%)[b]	K_i (nM)	MW (amu)	clogP	TPSA (Å^2)	CL_H (mL/min /kg)[c]	$P_{app,A\rightarrow B}$[d]	MDR[e]
8	(±)	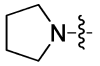	F	155 (n=7)	128	ND	369	3.0	79.4	13.5	ND	ND
8a	*S*	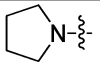	F	123 (n=2)[f]	147	<24 (n=4)	369	3.0	79.4	13.5	18.6	1.45
8b	*R*	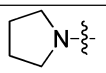	F	4690 (n=8)	114	5759 (n=2)	369	3.0	79.4	13.5	ND	1.60
9	(±)	H	F	>31600		ND	300	2.45	76.1	ND	ND	ND
10	(±)	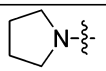	H	253	169	ND	351	2.75	79.4	12.1	ND	0.89
11	*S*	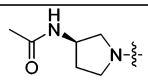	F	<10.0 (n=2)	143	ND	427	1.6	109	<5.0	3.93	12.1
12	(±)	Ph	F	3210 (n=7)	138	ND	376	4.34	76.1	<5.0	ND	ND
13	(±)	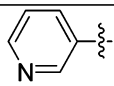	F	294	157	ND	377	2.9	89.0	6.35	22.0	0.84
14	(±)	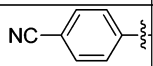	F	2640 (n=2)	124	ND	401	3.8	99.9	7.64	16.7	1.40
15	(±)	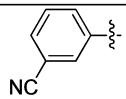	F	1850 (n=2)	156	ND	401	3.8	99.9	ND	15.1	1.17
16	(±)	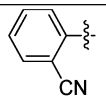	F	86.9	152	ND	401	3.8	99.9	8.81	12.9	1.16
16a	*S*	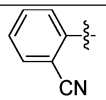	F	<10.0	ND	24 (n=1)	401	3.8	99.9	9.67	29.1	1.18

[a]mES, all values represent an average of a 9-point concentration−response curve run in triplicate. [b]mES, maximal efficacy was normalized to the average response to AMPA (100 μM) in the presence of cyclothiazide (32 μM), which was defined as 100%. [c]Predicted hepatic clearance (CL_H) from a human liver microsomal stability assay. [d]LC−MS/MS-based quantification of the absorptive apparent permeability ($P_{app,A\rightarrow B}$) of a potentiator (2 μM) across a population of Madin Darby Canine Kidney (MDCK) cells with reduced transporter expression. [e]The ratio of secretory ($P_{app,B\rightarrow A}$) to absorptive ($P_{app,A\rightarrow B}$) apparent permeabilities of a potentiator (2 μM) in human multidrug resistance protein-1-transfected MDCK cells (MDR1-MDCK). [f]This compound was tested in 4 other trials of the assay, but the data was excluded from the mean as the range of concentrations tested did not allow for either the asymptotic maximum or minimum to be achieved. ND = not determined.

(**13**) maintained fairly similar potency. As expected from the modeling and potency of **11**, nitrile introduction at the meta or para positions of the distal aromatic ring (**14** and **15**) produced very little improvement in activity, whereas incorporation into the ortho position (**16**) accessed the hydrophilic pocket and hence increased potency. As with the pyrollidine analogues, the *S*-enantiomer (**16a**) was more potent. Moreover, using the newly developed radioligand binding assay, the functional activity of compound **16a** is most likely attributed to its potent binding to the AMPAR potentiator site, which is apparent in the docked model of **16a** into the LBD (Figure 4). The enhanced potency of **16a** was complimented by its retention of

dx.doi.org/10.1021/jm401274b | J. Med. Chem. 2013, 56, 9180−9191

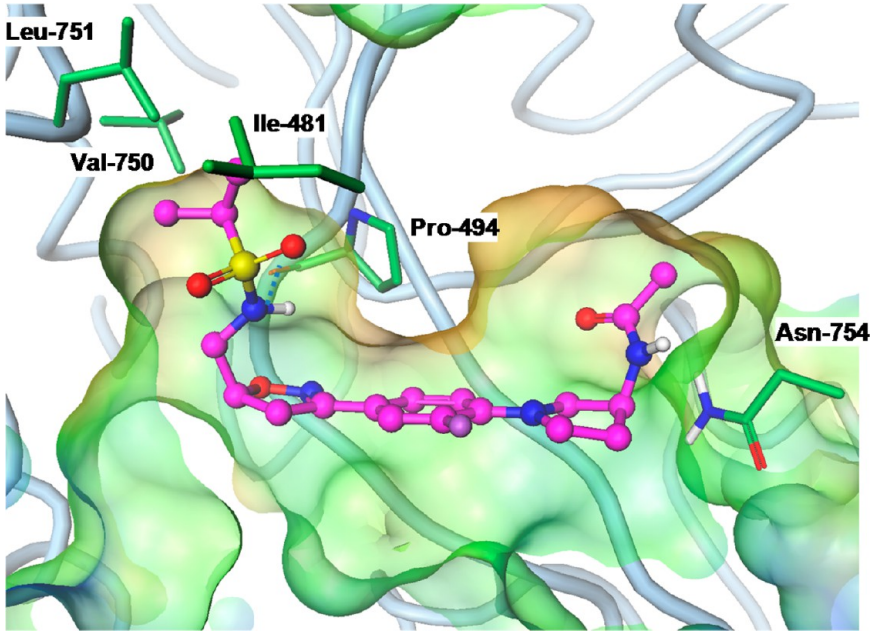

Figure 3. A 1.85 Å resolution X-ray cocrystal structure of **11** showing the second (symmetric) hydrophobic pocket occupied by the acetamide substituent off the 3-position on the pyrrolidine ring.

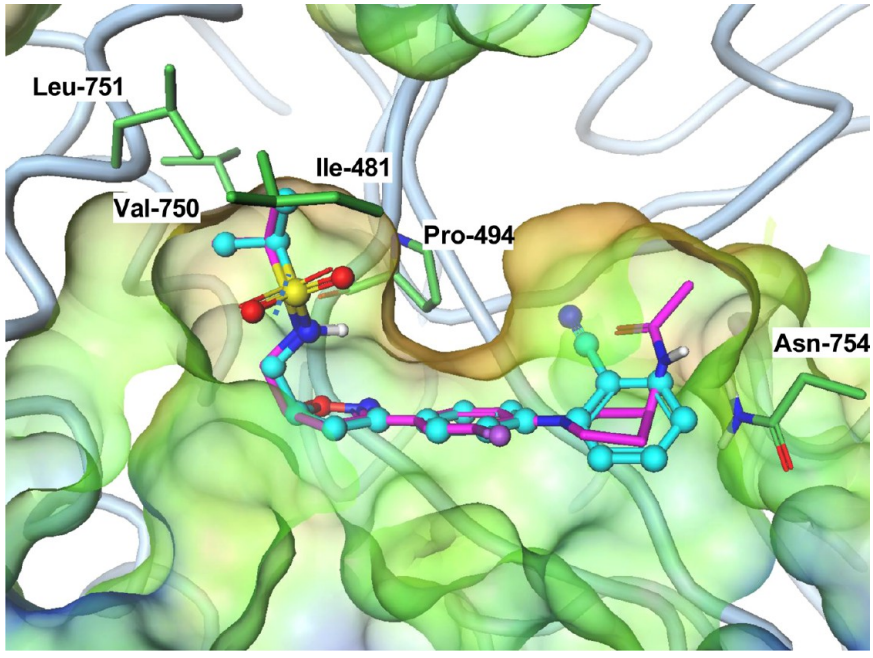

Figure 4. Model of **16a** aligned with the X-ray crystal structure of **11** to demonstrate the interaction of the cyano group. Like the acetamide of **11**, the *ortho*-nitrile of **16a** optimally accessed the symmetric hydrophilic pocket.

desirable physicochemical and in vitro ADME properties (Table 1).

Chemistry. Attractive features of the DHI series include its readily scalable synthesis and its rapidly expandable chemical landscape via enabled parallel synthesis of commercially available aldehydes (**17a–d**). Treatment of **17a–d** with hydroxylamine hydrochloride under basic conditions followed by reaction with *N*-chlorosuccinimide afforded chlorooximes **18a–d** in 90–99% yield (Scheme 1). The DHI core was prepared via a 3 + 2 cycloaddition between **18** and Boc-protected allyl amine in the presence of triethylamine to afford **19** in 85–90% yield. Liberation of the primary amine using TFA or HCl followed by addition of isopropyl sulfonyl chloride gave the desired sulfonamide **21** in 45–85% yield. An improved sequence, which eliminated the deprotection step, utilized allyl isopropylsulfonamide (**20**) in the 3 + 2 cycloaddition to cleanly afford the DHI core **21** in 85–90% yield. Suzuki couplings performed under standard conditions (Pd, ligand, base, and solvent; e.g., $Pd(PPh_3)_4$, Na_2CO_3, toluene/EtOH/H_2O) on the aryl bromide **21b** provided the biaryl series (**12–16**) and nucleophilic aromatic substitution on the aryl fluoride derivative (**21a** and **c**) provided the corresponding pyrrollidines (**8**, **10**, and **11**). As mentioned previously, enantiopure material could be obtained by either chiral preparative HPLC on the

dx.doi.org/10.1021/jm401274b | *J. Med. Chem.* 2013, 56, 9180–9191

Scheme 1. General Synthesis of the DHI Series[a]

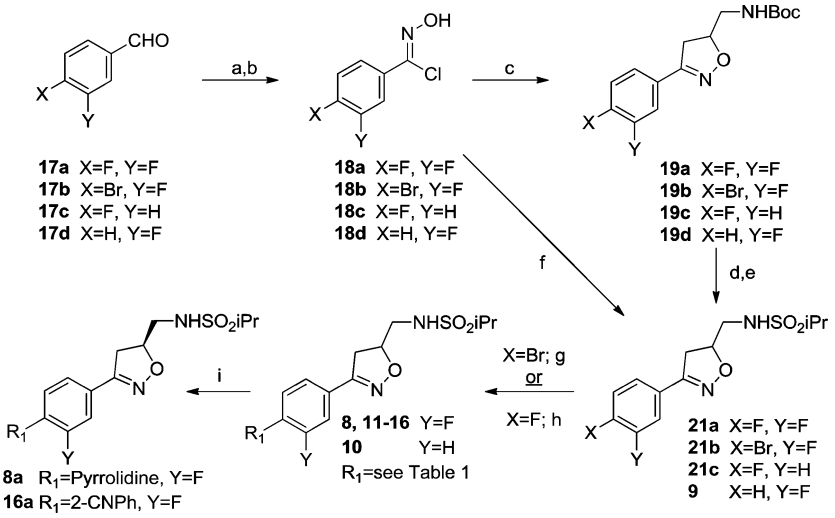

[a]Reagents and conditions: (a) $NH_2OH{\cdot}HCl$, NaOH, EtOH, 90−99%; (b) NCS, DMF, 92−99%; (c) Boc allylamine, Et_3N, 85−90%; (d) TFA, DCM, 75%; (e) isopropyl sulfonyl chloride, DBU, DMAP, 45−85% yield; (f) allylisopropylsulfonamide (**20**), Et_3N, DCM, RT, 20 h, 85−90%; (g) $Pd(PPh_3)_4$, Na_2CO_3, toluene/EtOH/H_2O, 80 °C, 20 h (Method A) or Xphos, $Pd(OAc)_2$, KF, 1:1 MeOH/toluene (Method B), 40−75%; (h) pyrrolidine, K_2CO_3, 20−70%; (i) chiral separations using SFC on either Chiralpak AD-H or Chiralcel OJ-H columns, 4.6 mm × 25 cm, carbon dioxide−methanol (90:10 or 80:20, v/v) at 2.5 mL/min, 30 °C, UV detection at 254 nm.

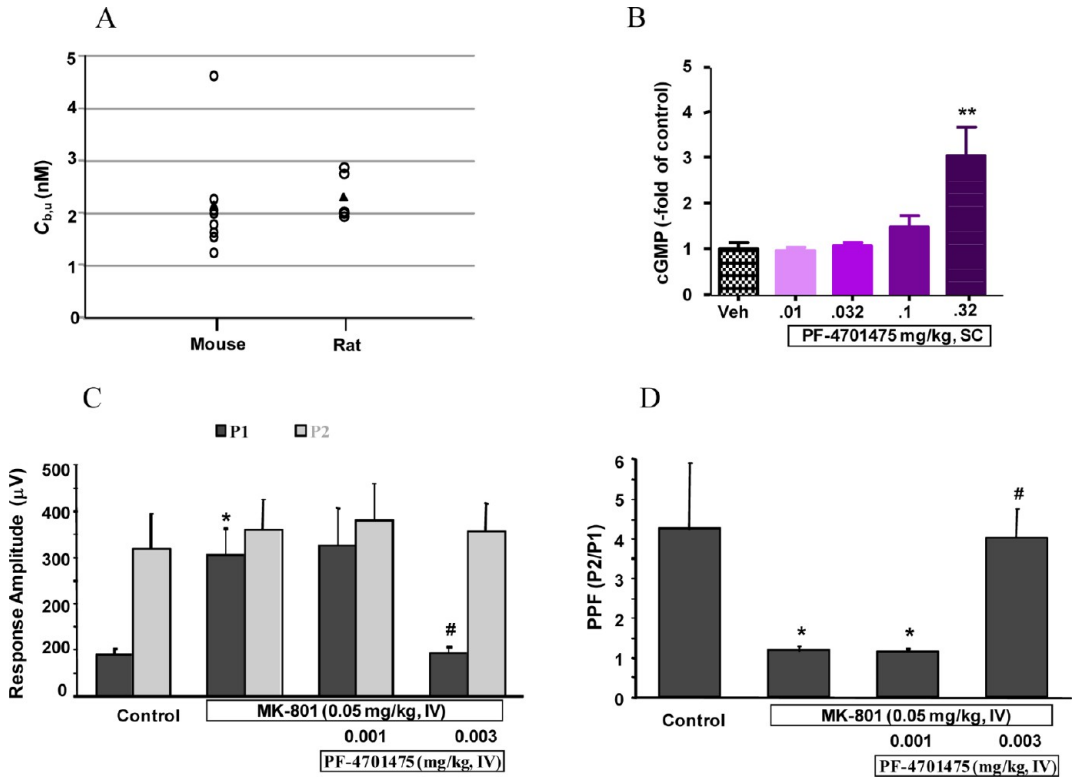

Figure 5. Summary of the AMPAR-mediated pharmacological characterization of **8a** in rodents. Panel A: Convulsion-causing $C_{b,u}$ in CD-1 mice (N = 8) and rats (N = 6); ○, individual animal; ▲, interanimal mean. Panel B: **8a** dose-dependently increased CD-1 mouse cerebellum cGMP; single doses were administered SC with a 0.5 h pretreatment time, with data expressed as mean ± SEM with N = 5−6/dose; ** $P < 0.01$, one-way ANOVA followed by post hoc Dunnett's t test. Panels C and D: Summary of the dose−response relationship in the rat MK-801-disrupted cortical oscillation (panel C) and paired-pulse facilitation (panel D) assay following IV administration of **8a**; * $P = 0.05$ vs control condition, # $P < 0.05$ vs MK-801 condition, two-tailed Student's t test.

final analogues or separation at the penultimate coupling intermediate. Unambiguous confirmation of the structure was achieved through X-ray crystallographic analysis of **8a** and penultimate intermediate **21**.

In Vivo Characterization of 8a. Upon its identification as the DHI prototype, **8a** was evaluated in a series of rodent assays to determine its neuropharmacokinetics and mechanism-mediated exposure−response relationships (Figure 5). By

dx.doi.org/10.1021/jm401274b | J. Med. Chem. 2013, 56, 9180−9191

integrating the free drug hypothesis,[31] the fact that interstitial fluid drug concentrations (C_{ISF}) dictate drug interaction with the extracellular ligand binding site of postsynaptic transmembrane proteins[32] and that unbound brain compound concentration ($C_{b,u}$) is a valid C_{ISF} surrogate,[33] a $C_{b,u}$-normalized AMPAR-mediated exposure−response continuum was defined for **8a** in rodents. This strategy provided a preliminary acute-dose rodent-based therapeutic index (TI) for **8a** in terms of its electrophysiological and biochemical effects relative to its convulsion threshold. Because of the known safety concerns of AMPAR overstimulation,[34a,b] defining the single-dose rodent-based TI of an AMPAR potentiator is a key step in its progression to large animal safety and efficacy studies for determining interspecies exposure−response relationships, which will ultimately dictate the compound's clinical viability.[35]

Compound **8a** had low unbound fractions in rat plasma (0.027) and brain homogenate (0.014). Using described methodology[33b] following a single subcutaneous (SC) dose (0.2 mg/kg) to Sprague−Dawley rats, **8a** demonstrated an identical terminal half-life (0.40 h) in both plasma and brain, an $AUC_{0-Tlast}$-derived total brain-to-total plasma compound concentration ratio (C_b:C_p) of 1.04, and a $C_{b,u}$-to-unbound plasma compound concentration ($C_{p,u}$) ratio ($C_{b,u}$:$C_{p,u}$) of 0.54. Consistent with it being a highly permeable compound that is not a substrate for P-gp (Table 1) or breast cancer resistance protein (Pfizer, internal unpublished data), **8a** has net equilibrium at the blood−brain barrier in rats, which likely occurs in higher-order species.[33b]

In CD-1 mice, general convulsions, occurring from 5 to 11 min postdose, were observed at both 0.32 (N = 2 of 6 animals) and 0.56 (N = 6/6) mg/kg, SC and corresponded to a mean (±SD) convulsion-causing $C_{b,u}$ of 2.1 ± 1.1 nM. In Sprague−Dawley rats, convulsions, occurring from 13 to 23 min postdose, were observed in both the 0.32 (N = 1/5) and 0.56 (N = 5/5) mg/kg, SC groups at a mean $C_{b,u}$ of 2.3 ± 0.4 nM. In rats, generalized tremors began in all animals ca. 10 min before full convulsion. Collectively (Figure 5A), **8a** had an essentially identical exposure-based convulsion threshold in both rats and mice.

Employing a modified version of a cerebellum cyclic guanosine monophosphate (cGMP) assay,[36] **8a** increased cGMP levels in CD-1 mouse cerebellum with statistically significant elevations (P < 0.01, versus vehicle-treated animals) 0.5 h after receiving 0.32 mg/kg, SC (Figure 5B) at a mean $C_{b,u}$ of 0.4 nM. The effects of **8a** on neurocircuitry function were quantified in urethane-anesthetized Sprague−Dawley rats following disruption of the cortical electroencephalogram and paired-pulse facilitation (PPF) by the NMDA receptor antagonist MK-801.[37] This model, grounded in the NMDA receptor hypofunction hypothesis of schizophrenia,[38] evaluates a compound's ability to affect the monosynaptic projection from the hippocampus/subiculum to the medial prefrontal cortex that contributes to working memory,[39] and such dysfunction is implicated in the decreased cognitive performance of schizophrenia patients.[40] Intravenous bolus (IV) administration of **8a** at 0.003 mg/kg, but not 0.001 mg/kg, significantly reversed the MK-801-induced increase in the low delta component of the local field potential (Figure 5C) and decrease in PPF (Figure 5D). After the 0.003 mg/kg bolus, these significant effects of **8a** began at ca. 5 min at a projected $C_{b,u}$ of 0.004 nM based on linear dose−$C_{b,u}$ extrapolation from a rat IV pharmacokinetics study (0.01 mg/kg). Holistically, the in vivo data suggest that increasing **8a** $C_{b,u}$ progresses sequentially to initial nootropic electrophysiological effects ca. 100-fold below cerebellar cGMP elevation, which occurs ca. 5-fold below generalized convulsion. From an acute-dose perspective, **8a** has a ca. 500-fold TI for convulsion relative to pro-cognitive pharmacodynamics in rats. These rat-based efficacy data, coupled with projected human pharmacokinetic parameters and assuming both the translatability of the rodent exposure−response relationship and no compression of the reported acute dose-based TI upon chronic administration, suggest a daily clinically efficacious dose of ca. 0.2 mg for **8a**.[41]

CONCLUSIONS

A novel series of AMPAR potentiators with a DHI core was identified by a functional assay using mES cell-derived neurons. The impact on binding of various functional groups of the lead structure **7** was determined using SBDD aided by X-ray crystal structures of select AMPAR potentiators docked within the human GluA2o LBD. Series optimization to increase functional potency led to the identification of **11** whose tritiated form helped develop a proprietary radioligand binding assay for measuring potentiator binding to native AMPARs in rat cortical tissue. Simultaneously through a minimal number of design cycles, **8a** was identified for in vivo AMPAR-mediated pharmacological characterization in rodents, which suggested its exposure separation between desired and deleterious effects was sufficient for its preclinical progression. Finally, SBDD-guided optimization of primary pharmacology, with consideration of the physicochemical and in vitro ADME properties favorable for orally administered, brain-penetrant drugs, led to the discovery of **16a**, which showed that the potentially bioactivatable aniline within **8a** was not required for highly potent compounds.

EXPERIMENTAL SECTION

General Chemistry Procedure. All reagents and solvents were used as purchased from commercial sources. Reactions were carried out under nitrogen. Mass spectral data was collected on a Micromass ADM atmospheric pressure chemical ionization instrument (LRMS APCI). NMR spectra were generated on a Varian 400 and 500 MHz or Bruker 400 MHz instruments. Chemical shifts were recorded in ppm relative to tetramethylsilane (TMS) with multiplicities given as s (singlet), bs (broad singlet), d (doublet), t (triplet), dd (doublet of doublets), dt (double of triplets), and m (multiplet). High-resolution mass spectra (HRMS) Accurate Mass Spectrometry analyses were conducted on an Agilent 6220 TOF mass spectrometer (Agilent Technologies, Wilmington, DE) in positive on a Agilent ZORBAX, 3.0 mm × 50 mm, C18, 1.8 μm; Column Temperature 60 °C or negative on a Waters XBridge, 3.0 mm × 50 mm, C18, 2.5 μm; Column Temperature 60 °C in electrospray mode. The system was calibrated to greater than 1 ppm accuracy across the mass range prior to analyses according to manufacturer's specifications. The samples were separated using UHPLC on an Agilent 1200 system prior to mass spectrometric analysis. The resulting spectra were automatically lockmass corrected and the target mass ions and any confirming adducts (Na^+, NH_4^+) were extracted and combined as a chromatogram. The mass accuracy was calculated for all observed isotopes against the theoretical mass ions derived from the chemical formula using MassHunter software (Agilent Technologies). Low resolution mass spectra were determined on a Waters/Micromass system. The X-ray diffraction measurements were carried out at 298 K on a Bruker SMART APEX CCD area detector system equipped with a graphite monochromator and sealed tube Cu radiation (1.54178 Å) source. Compound purity was determined by combustion analysis (Quantitative Technologies Inc.) where the analyses indicated by the symbols of the elements were within ±0.4% of the theoretical values or by high pressure liquid chromatography (HPLC) confirming it to be ≥95% or

by a combination of the two methods. HPLC conditions utilized are as follows. Gradient: 0−1.5 min 5% acetonitrile (ACN)/water, 1.5−10 min 5−100% ACN/water, 10−11 min 100% ACN, 11−12.5 min 100−5% ACN/water; UV detector, 254 nM. Retention times (RT) are in minutes and purity is calculated as % total area. (Column: XBridge C18 5 μ (4.6 mm × 150 mm); mobile phase, flow rate of 1.5 mL/min with solvent containing 0.1% TFA.

Compound **8a**, >99% chemical purity, Supplemental Data) and *N*-((*S*)-1-(3,5-[3*H*]-2-fluoro-4-((*S*)-5-((1-methylethylsulfonamido)-methyl)-4,5-dihydroisoxazol-3-yl)phenyl)pyrrolidin-3-yl)acetamide ([^{3}H]**11**), 98.5% radiochemical purity, 100% ee, 49 Ci/mmol) were synthesized and fully characterized by Neuroscience Chemistry at Pfizer Worldwide Research and Development (WRD, Groton, CT). Compound **8a** (Product No. PZ0215) and **11** (Product No. PZ0216) are commercially available from Sigma-Aldrich Corporation (St. Louis, MO).

General Procedure for the SN_2Ar. The dihydroisoxazole **21** (3.1 mmol), the corresponding pyrrolidine (17.6 mmol), and powdered potassium carbonate (4.0 mmol) were combined in a sealed tube and heated to 135−140 °C. The resulting melt was heated until the starting dihydroisoxazole was consumed (2−16 h depending on substrate). The reaction mixture was cooled to room temperature, diluted with water (10 vol), and extracted with ethyl acetate (3 × 10 vol). The combined organic layers were washed consecutively with water (2 × 10 vol), saturated sodium chloride solution (10 vol), dried over anhydrous magnesium sulfate and filtered. The solvent was removed under reduced pressure and the resulting solid purified via chromatography or crystallization to afford the desired product.

*N-((3-(3-Fluoro-4-(pyrrolidin-1-yl)phenyl)-4,5-dihydroisoxazol-5-yl)methyl)propane-2-sulfonamide (**8**).* The product was obtained from **21a** and pyrrolidine. The crude material was purified via flash chromatography (Isco silica gel, 5% MeOH/DCM) followed by crystallization from toluene to afford **8** in 78% yield as a white crystalline solid. ^{1}H NMR (400 MHz, $CDCl_3$) δ 7.32 (dd, J = 14.93, 2.07 Hz, 1H), 7.21 (dd, J = 8.30, 2.07 Hz, 1H), 6.61 (t, J = 8.92 Hz, 1H), 4.79−4.89 (m, 1H), 4.67 (t, J = 6.43 Hz, 1H), 3.15−3.52 (m, 9H), 1.93−2.01 (m, 4H), 1.38 (dd, J = 6.84, 2.28 Hz, 6H).

Separation of the enantiomers was done via a chiral chromatography (SFC chromatography on either Chiralcel OJ-H column, 4.6 mm × 25 cm, carbon dioxide−methanol (90:10 or 80:20, v/v) at 2.5 mL/min, 30 °C, UV detection at 254 nM) to afford (**8a** and **8b**) as white solids.

Enantiomer 1: ^{1}H NMR (400 MHz, $CDCl_3$) δ 7.32 (dd, J = 14.93, 2.07 Hz, 1H), 7.22 (dd, J = 8.30, 2.07 Hz, 1H), 6.60 (t, J = 8.92 Hz, 1H), 4.80−4.88 (m, 1H), 4.57 (t, J = 6.43 Hz, 1H), 3.45−3.51 (m, 4H), 3.16−3.44 (m, 5H), 1.94−2.01 (m, 4H), 1.38 (dd, J = 6.64, 2.49 Hz, 6H). HRMS (ESI-) m/z: [M + H]$^+$ Calcd for $C_{17}H_{25}FN_3O_3S$ 370.1595; found 370.1598.

Enantiomer 2: ^{1}H NMR (400 MHz, $CDCl_3$) δ 7.33 (dd, J = 15.14, 1.87 Hz, 1H), 7.22 (dd, J = 8.30, 2.07 Hz, 1H), 6.61 (t, J = 8.71 Hz, 1H), 4.80−4.89 (m, 1H), 4.52 (t, J = 6.22 Hz, 1H), 3.45−3.51 (m, 5H), 3.15−3.45 (m, 5H), 1.95−2.01 (m, 4H), 1.39 (dd, J = 6.84, 2.28 Hz, 6H). Calcd. for $C_{17}H_{24}FN_3O_3S$: C, 55.27; H, 6.33; N,11.37. Found: C, 55.24; H, 6.78; N, 11.58. HRMS (ESI-) m/z: [M + H]$^+$ Calcd for $C_{17}H_{25}FN_3O_3S$ 370.1595; found 370.1597.

*N-((3-(4-(Pyrrolidin-1-yl)phenyl)-4,5-dihydroisoxazol-5-yl)-methyl)propane-2-sulfonamide (**10**).* The product was obtained from **21c** and pyrrolidine. The crude material was purified via flash chromatography (Isco silica gel, 10% MeOH/DCM) to afford the product in 22% yield as an off-white solid. ^{1}H NMR (400 MHz, $CDCl_3$) δ 7.49−7.54 (m, 2H), 6.51−6.57 (m, 2H), 4.78−4.87 (m, 1H), 4.55 (t, J = 6.22 Hz, 1H), 3.15−3.50 (m, 9H), 2.03 (td, J = 6.64, 3.32 Hz, 4H), 1.37−1.41 (m, 6H). Calcd for $C_{17}H_{25}N_3O_3S$: C, 58.09; H, 7.17; N, 11.96. Found: C, 57.62; H, 7.15; N, 11.71. HRMS (ESI-) m/z: [M + H]$^+$ Calcd for $C_{17}H_{26}N_3O_3S$ 352.1689; found 352.1684.

*N-((3S)-1-(2-Fluoro-4-(5-((1-methylethylsulfonamido)methyl)-4,5-dihydroisoxazol-3-yl)phenyl)pyrrolidin-3-yl)acetamide (**11**).* The product was obtained from **21a** and commercially available (*S*)-*N*-(pyrrolidin-3-yl)acetamide. The crude material was crystallized from toluene to afford the product in 68% yield as a white solid. ^{1}H NMR (400 MHz, $CDCl_3$) δ 7.36 (dd, J = 14.93, 2.07 Hz, 1H), 7.24 (dd, J = 8.50, 1.87 Hz, 1H), 6.63 (t, J = 8.71 Hz, 1H), 5.80 (d, J = 7.05 Hz, 1H), 4.81−4.91 (m, 1H), 4.49−4.67 (m, 2H), 3.60−3.75 (m, 2H), 3.47 (ddd, J = 13.79, 5.91, 3.53 Hz, 2H), 3.29−3.42 (m, 3H), 3.16−3.28 (m, 2H), 2.28 (dd, J = 13.89, 5.60 Hz, 1H), 2.00 (s, 3H), 1.92−1.99 (m, 1H), 1.38 (dd, J = 6.84, 3.53 Hz, 6H). Calcd for $C_{19}H_{27}FN_4O_4S$: C, 53.51; H, 6.38; N, 13.14. Found: C, 53.51; H, 6.38; N, 13.09. HRMS (ESI-) m/z: [M + H]$^+$ Calcd for $C_{19}H_{28}FN_4O_4S$ 427.1810; found 427.1805.

General Procedure for the Suzuki Coupling. *Method A.* Sodium carbonate (0.25 mmol) was added to a solution of the bromide **21b** (0.05 mmol) in ethanol (1.0 mL) and water (0.2 mL). The solution was degassed for 15 min and a solution of $Pd(PPh_3)_4$ (2.5 μmol) in toluene (0.1 mL) was added. The reaction mixture was heated to 80 °C and stirred for 20 h. The reaction mixture was cooled to room temperature and partitioned between ethyl acetate (3 × 2.5 mL) and 1 N sodium hydroxide (1.5 mL). The organic layer was washed with saturated sodium chloride solution, dried over anhydrous sodium sulfate, and the solvent removed under reduced pressure. The crude product was purified by column chromatography.

Method B. Bromide **21b** (0.53 mmol), Xphos (0.05 mmol), KF (2.67 mmol), boronic acid (0.80 mmol), and palladium acetate (0.025 mmol) were combined in a 10 mL microwave vial. The vial was purged with N_2/vacuum three times then a degassed 1:1 MeOH/toluene solution (2 mL) was added and heated at 130 °C for 50 min in the microwave. The solvent was removed under reduced pressure and diluted with saturated sodium bicarbonate (25 mL) and washed with dichloromethane (3 × 25 mL). The combined organic layers were dried over anhydrous magnesium sulfate and the solvent removed under reduced pressure. The crude product was purified by column chromatography.

*N-((3-(2-Fluoro-[1,1′-biphenyl]-4-yl)-4,5-dihydroisoxazol-5-yl)-methyl)propane-2-sulfonamide (**12**).* Prepared via Method A from **21b** and phenylboronic acid in 46% yield as an off white solid. ^{1}H NMR (400 MHz, $CDCl_3$) δ 7.53−7.59 (m, 2H), 7.37−7.52 (m, 6H), 4.95 (dddd, J = 10.68, 7.36, 5.39, 3.53 Hz, 1H), 4.80 (t, J = 6.43 Hz, 1H), 3.28−3.56 (m, 4H), 3.15−3.27 (m, 1H), 1.36−1.42 (m, 6H).

*N-((3-(3-Fluoro-4-(pyridin-3-yl)phenyl)-4,5-dihydroisoxazol-5-yl)-methyl)propane-2-sulfonamide (**13**).* Prepared via Method A from **21b** and pyridin-3-ylboronic acid in 76% yield as an off white solid. ^{1}H NMR (400 MHz, $CDCl_3$) δ 8.83 (br. s., 1H), 8.66 (d, J = 3.90 Hz, 1H), 7.95 (dd, J = 7.80, 1.56 Hz, 1H), 7.40−7.60 (m, 4H), 4.91−5.06 (m, 1H), 4.64 (t, J = 6.24 Hz, 1H), 3.29−3.60 (m, 4H), 3.23 (td, J = 13.66, 6.83 Hz, 1H), 1.34−1.45 (m, 6H). Calcd for $C_{18}H_{20}FN_3O_3S{\cdot}1.6\ H_2O$: C, 53.22; H, 5.76; N, 10.34. Found: C, 53.05; H, 5.02; N, 10.20. HRMS (ESI-) m/z: [M + H]$^+$ Calcd for $C_{18}H_{20}FN_3O_3S$ 378.1282; found 378.1285.

*N-((3-(4′-Cyano-2-fluoro-[1,1′-biphenyl]-4-yl)-4,5-dihydroisoxazol-5-yl)methyl)propane-2-sulfonamide (**14**).* Prepared via Method B from **21b** and (4-cyanophenyl)boronic acid in 76% yield as an off white solid. ^{1}H NMR (400 MHz, $CDCl_3$) δ 7.73−7.81 (m, 2H), 7.64−7.72 (m, 2H), 7.44−7.60 (m, 3H), 4.98 (dd, J = 4.98, 3.32 Hz, 1H), 4.54 (dd, J = 7.05, 5.81 Hz, 1H), 3.32−3.58 (m, 4H), 3.22 (quin, J = 6.84 Hz, 1H), 1.40 (dd, J = 6.84, 3.94 Hz, 6H). HRMS (ESI-) m/z: [M + H]$^+$ Calcd for $C_{20}H_{21}FN_3O_3S$ 402.1282; found 402.1286.

*N-((3-(3′-Cyano-2-fluoro-[1,1′-biphenyl]-4-yl)-4,5-dihydroisoxazol-5-yl)methyl)propane-2-sulfonamide (**15**).* Prepared via Method B from **21b** and (3-cyanophenyl)boronic acid in 45% yield as a tan solid. ^{1}H NMR (400 MHz, $CDCl_3$) δ 7.86 (d, J = 1.24 Hz, 1H), 7.81 (qd, J = 7.88, 1.52 Hz, 1H), 7.70 (td, J = 7.88, 1.45 Hz, 1H), 7.44−7.62 (m, 4H), 4.97 (dddd, J = 10.73, 7.73, 4.77, 3.32 Hz, 1H), 4.51−4.58 (m, 1H), 3.31−3.58 (m, 4H), 3.22 (spt, J = 6.80 Hz, 1H), 1.40 (dd, J = 6.64, 3.73 Hz, 6H). Calcd. for $C_{20}H_{20}FN_3O_3S$: C, 59.84; H, 5.02; N, 10.47. Found: C, 59.24; H, 5.17; N, 10.09. HRMS (ESI-) m/z: [M + H]$^+$ Calcd for $C_{20}H_{21}FN_3O_3S$ 402.1282; Found 402.1283.

*N-((3-(2′-Cyano-2-fluoro-[1,1′-biphenyl]-4-yl)-4,5-dihydroisoxazol-5-yl)methyl)propane-2-sulfonamide (**16**).* Prepared via Method B from **21b** and (2-cyanophenyl)boronic acid in 38% yield as an off white solid. ^{1}H NMR (400 MHz, $CDCl_3$) δ 7.80 (dd, J = 7.88, 1.24 Hz, 1H), 7.66−7.72 (m, 1H), 7.46−7.58 (m, 5H), 4.97 (dddd, J =

dx.doi.org/10.1021/jm401274b | J. Med. Chem. 2013, 56, 9180−9191

10.68, 7.36, 5.60, 3.32 Hz, 1H), 4.69 (t, J = 6.43 Hz, 1H), 3.29−3.56 (m, 4H), 3.23 (spt, J = 6.84 Hz, 1H), 1.40 (dd, J = 6.84, 2.70 Hz, 6H). Calcd. for $C_{20}H_{20}FN_3O_3S$: C, 59.84; H, 5.02; N, 10.47. Found: C, 59.25; H, 4.95; N, 10.23. HRMS (ESI-) m/z: $[M + H]^+$ Calcd for $C_{20}H_{21}FN_3O_3S$ 402.1282; found 402.1281.

Separation of **16** was performed via a chiral chromatography (SFC chromatography on a Chiralpak AD-H column, 4.6 mm × 25 cm, carbon dioxide−methanol (90:10 or 80:20, v/v) at 2.5 mL/min, 30 °C, UV detection at 254 nM) to afford (**16a**) as a white solid. ^{1}H NMR (400 MHz, $CDCl_3$) δ 7.77−7.82 (m, 1H), 7.65−7.72 (m, 1H), 7.44−7.58 (m, 5H), 4.86−5.01 (m, 2H), 3.29−3.56 (m, 4H), 3.17−3.27 (m, 1H), 1.39 (dd, J = 6.84, 3.53 Hz, 6H). HRMS (ESI-) m/z: $[M + H]^+$ Calcd for $C_{20}H_{21}FN_3O_3S$ 402.1282; found 402.1289.

X-ray Crystallography. GluR2-S1S2J flop protein was expressed, refolded, and purified essentially as previously reported[27b] with 1 mM (*S*)-Glu present during all steps. It was crystallized in complex with (*S*)-Glu and potentiator compounds by the hanging-drop vapor-diffusion method at 4 °C. The protein solution contained 7 mg/mL GluR2-S1S2J, 10 mM (*S*)-Glu, 10 mM HEPES (pH 7.5), 20 mM NaCl, and 1 mM EDTA. Compound was added to a final concentration of 150 μM from a 30 mM DMSO stock. To this solution, an equal amount of reservoir solution containing 10% PEG 8000, 0.1 M ZnAc, and 0.1 M NaAc, pH 5.5, was added, and 2 μL drops of this mixture were allowed to equilibrate by vapor diffusion over a 1 mL reservoir. Crystals appeared in the drops in 3−5 days, were transferred to a cryoprotectant solution consisting of the crystallization buffer supplemented with 15% glycerol, and flash-frozen in liquid nitrogen. Because the modulators bind on the molecular 2-fold axis, two modulator molecules were modeled for each binding site, each with occupancies of 0.5. Data collection and refinement statistics are provided in the Supporting Information.

Rat Brain Homogenate Radioligand Binding Assay. Brains from 7 to 8 week old Sprague−Dawley rats were purchased from Pel-Freez Biologicals (Rogers, AR) and stored at −80 °C. The cortex was dissected, homogenized using a polytron in 50 mM Tris 7.4 and centrifuged (40,000g for 20 min). The resulting pellet was resuspended in 50 mM Tris 7.4 and centrifuged (40,000g for 20 min); this was repeated three times for a total of 4 washes, after which the pellet was resuspended in 30 mM Tris 7.4 at 100 mg/mL and stored at −80 °C. The multiple wash steps were performed to remove endogenous glutamate from the cortical tissue preparation.

Saturation binding studies were performed by adding 175 μL of different concentrations of **11** in assay buffer (30 mM Tris HCl, pH 7.4) to a 96-well polypropylene plate. Twenty-five microliters of assay buffer or *N*-((3*R*,4*S*)-3-(2′-cyano-[1,1′-biphenyl]-4-yl)tetrahydro-2*H*-pyran-4-yl)propane-2-sulfonamide (**22**, PF-04697190)[41] was then added to each well. Compound **22** (100 μM in assay buffer, final concentration 10 μM) was used to determine nonspecific binding. L-Glutamic acid (25 μL, 5 mM stock concentration, 500 nM final concentration) was added to each well unless indicated. The previously prepared rat cortical tissue was thawed and homogenized (100 mg/mL), then added (25 μL, 2.5 mg tissue, 0.25 mg/well final concentration) to each sample well. Plates were incubated for 2 h at 37 °C and then harvested onto uncoated Filtermat B filters (PerkinElmer Inc., Waltham, MA) using a Skatron filter harvester (Skatron Instruments Ltd., Newmarket, UK) and Tris wash buffer (50 mM, pH 7.4, 4 °C). Filters were dried overnight at room temperature, placed in scintillant bags and read using a Betaplate filtermat reader (PerkinElmer, Inc.).

Competition binding studies used similar methods. Compound **11** was added to each well (175 μL) at a concentration of approximately 1 nM; for each experiment, the precise stock solution concentration was determined by liquid scintillation counting. L-Glutamic acid (25 μL) was added. Assay buffer, test compounds, or **22**[41] were added (25 μL) to negative control, sample, and positive control wells, respectively. Test compounds for competitive binding experiments were prepared as DMSO stock solutions (10 or 30 mM), then titrated for dose response studies, at 10-fold their final concentrations. Concentration−response data were fitted using a logistic four parameter fit model. The K_i for each compound was determined using the calculated IC_{50} and the ligand concentration determined for each experiment using the Cheng−Prusoff equation.

In Vivo Studies with 8a. Chemicals and solvents were supplied by Sigma-Aldrich Corporation (St. Louis, MO), Thermo Fisher Scientific (Waltham, MA), and Mallinckrodt Baker, Inc. (Phillipsburg, NJ). For control matrices, species-specific plasma was procured from Bioreclamation, Inc. (Hicksville, NY) and rat brain tissue was obtained at WRD. Male CD-1 mice and Sprague−Dawley rats were bought from Harlan Laboratories (Indianapolis, IN) or Charles River Laboratories, Inc. (Wilmington, MA), respectively. All studies were performed in accordance with the *Guide for the Care and Use of Laboratory Animals* (Institute of Laboratory Animal Resources, 1996) using protocols reviewed and approved by the WRD Institutional Animal Care and Use Committee. All blood samples were collected into EDTA-containing tubes and processed immediately to obtain plasma, and the collection of neuromatrices followed published techniques.[33b] All biomatrices collected for **8a** quantification, which occurred using a described method,[41] were stored at −70 °C until processing for bioanalysis.

Plasma and Brain Homogenate Nonspecific Binding. Using a reported equilibrium dialysis procedure,[33b] the unbound fraction (f_u) of **8a** (1 μM, N = 4/matrix) was determined in Sprague−Dawley rat plasma ($f_{u,p}$) and brain homogenate ($f_{u,b}$). The stability of **8a** in each biomatrix and the optimal dialysis time were determined separately prior to actual studies.

In Vivo Pharmacokinetics. Before in vivo pharmacology experiments, studies with **8a** characterizing its pharmacokinetics (peripheral and/or central) were conducted in rodents to determine total plasma (C_p) and/or brain (C_b) compound concentrations at select times after a specific dose, which allowed the correlation of pharmacodynamics to C_p and/or C_b in in vivo pharmacology experiments. Individual animal doses were calculated based on respective dose solution concentrations (mg/mL), pretreatment body weights (kg), and dose volume (mL/kg); the actual amount of dose solution administered to each animal was determined by weighing the loaded syringe before and after it was dispensed. All study animals were fasted overnight.

Mouse. A single dose (0.1 mg/kg) of **8a** in 5:5:90 (v/v/v) DMSO/cremophor EL/deionized H_2O (0.01 mg/mL) was administered (10 mL/kg) subcutaneously (SC) to CD-1 (N = 2) mice. At 0.5 h postdose, animals were placed under isoflurane anesthesia for the collection of blood and brain samples.

Rat Intravenous Dose. From jugular vein-cannulated Sprague−Dawley rats (N = 3) receiving a single bolus (1 mL/kg) intravenously (IV) of **8a** (0.01 mg/kg) in 2:98 (v/v) DMSO/10% hydroxypropyl-β-cyclodextrin, blood samples (0.5 mL) were serially collected just before dosing and at 0.083, 0.25, 0.5, 1, 2, 4, 6, 8, and 12 h postdose.

Neuropharmacokinetics. Applying described methodology,[33b] a single dose (0.2 mg/kg, SC) of **8a** in 20% hydroxypropyl-β-cyclodextrin (0.2 mg/mL) was injected (1 mL/kg) into each male Sprague−Dawley rat. Blood, cerebrospinal fluid (CSF), and brain samples were collected from each animal after euthanasia by CO_2 asphyxiation at 0.25, 0.5, 1, 2, 4, and 8 h postdose (N = 2/time point).

Pharmacokinetic parameters were calculated by noncompartmental analyses using WinNonlin version 5.2 (Pharsight Corp., Mountain View, CA). The area under the matrix compound concentration−time curve ($AUC_{0-Tlast}$) was calculated using the linear trapezoidal method, the elimination rate constant (k_{el}) was determined by linear regression of the log concentration versus time data during the last observable elimination phase, and half-life ($t_{1/2}$) was calculated as $0.693/k_{el}$. Both C_{max} and T_{max} were taken directly from the matrix compound concentration versus time data, and $AUC_{0-Tlast}$-based interneurocompartmental ratios were calculated.[33b]

In select rodent pharmacology models, **8a** was studied to understand the relationship between its $C_{b,u}$ and a particular AMPAR-mediated effect, which together allowed comparison to its in vitro pharmacology values. Collectively, this strategy provided dose-dependent, temporally normalized, and assay-dependent $C_{b,u}$ that could be directly compared across all in vivo models. For each species, its pharmacodynamics evaluation used the same dosing vehicle, volume, and route as its pharmacokinetics studies. For terminal assays

in which brain tissue was collected from an animal undergoing the assessment (i.e., convulsion dose–response), $C_{b,u}$ (nM units) was determined by measured C_b, **8a** MW (369.5 g/mol), rat $f_{u,b}$, an assumed brain tissue density of 1 g/mL, and eq 1:

$$(C_b/\mathrm{MW})\cdot 1000\cdot f_{u,b} = C_{b,u} \quad (1)$$

The experimentally determined rat $f_{u,b}$ was used for mouse $C_{b,u}$ calculations since interspecies $f_{u,b}$ are highly consistent.[34c]

For assays (i.e., mouse cGMP and rat PPF) in which plasma or brain samples were not collected for **8a** quantification from animals undergoing pharmacodynamic evaluation, the $C_{b,u}$ for each tested dose at a fixed time point was projected assuming stationary pharmacokinetics within the dose range studied either directly from the mouse SC pharmacokinetics dose-C_b data (mouse cGMP) or indirectly via eq 2 and the rat IV pharmacokinetics dose-derived C_p-time data (rat PPF):

$$(C_p/\mathrm{MW})\cdot 1000\cdot f_{u,p}(C_{b,u}{:}C_{p,u}) = C_{b,u} \quad (2)$$

Within eq 2, $C_{b,u}$:$C_{p,u}$ is the AUC-based interneurocompartmental relationship determined in the rat neuropharmacokinetics study that allows the projection of $C_{b,u}$ from a measured C_p.[33b]

Convulsion Dose–Response Studies. Compound **8a** was administered to adult male CD-1 mice (0.32 or 0.56 mg/kg, SC; N = 6/dose) or Sprague–Dawley rats (0.32 or 0.56 mg/kg, SC; N = 5/dose), which were observed for up to 1.5 h postdose. Individual animals were euthanized by CO_2 asphyxiation at the time of convulsion (if any), and blood and brain were collected for **8a** quantification.

Mouse Cerebellum Cyclic Guanosine Monophosphate (cGMP) Assay. Paralleling the procedure of Ryder et al.,[36] adult male CD-1 mice (25–30 g, acclimated to the vivarium 7 d before use, N = 5–6/dose) receiving vehicle or **8a** (0.01, 0.032, 0.1, or 0.32 mg/kg, SC) were placed in an open shoebox with sawdust bedding and observed for 0.5 h. Mice were then individually placed head first in a Plexiglas restraining device and euthanized using a beam of microwave radiation focused on the skull for 0.88 s at 100% power in a Cober Electronics microwave (Cober Electronics, Inc., Norwalk, CT). After cooling for 1 min, the cerebellum was dissected, weighed, and frozen on dry ice. Tissue cGMP levels were determined using a competitive enzyme immunoassay (EIA) using a commercially available Cyclic GMP EIA kit (Cayman Chemical Company, Ann Arbor, MI). All buffers and cGMP standards were prepared exactly as described in the package insert. Each cerebellum sample was homogenized (10 μL buffer/mg tissue) in lysis buffer (10 mM Tris HCl, 100 mM NaCl, 1 mM EDTA, and 0.3% NP-40, pH 7.4) using a tip sonicator. Homogenate was added to a 1.5 mL Eppendorf tube and centrifuged (18,000*g* for 20 min at 4 °C), and the supernatant was diluted 1:25 with EIA buffer and added in triplicate to a 96-well plate. Samples were processed according to kit directions for 12 h at 4 °C. A cGMP standard curve (0.023 to 3.0 pmol/mL) was included on each assay plate. Following incubation, plates were washed, developed using Ellman's reagent for 2 h at rt, and then read at 420 nm on a SpectraMax Microplate Reader (Molecular Devices, LLC). Data were compiled and reduced using the SpectraMax data reduction software, which calculates sample cGMP levels via standard curve extrapolation. For each dose group, data were reported as group means ± SEM using X-fold changes in tissue cGMP levels relative to the vehicle-treated group. Doses of **8a** were compared to the concurrent vehicle control group using One-way Analysis of Variance (ANOVA) followed by Dunnett's t test (SigmaStat Version 3.5; Systat Software, Inc., Chicago, IL). A value of $p < 0.05$ indicated a statistically significant effect.

Rat MK-801-Disrupted Cortical Oscillation and Paired-Pulse Facilitation (PPF) Assay. The objective of this study was to quantify the effects of systemically administered **8a** on the cortical disruption of electroencephalogram (EEG) and paired-pulse facilitation (PPF) by the noncompetitive NMDAR antagonist MK-801 in urethane-anesthetized Sprague–Dawley rats. This is a preclinical model, which evaluates the subiculum-medial prefrontal cortex pathway, proposed for studying NMDAR hypofunction of schizophrenia. Experimental procedures were those published by Kiss et al.[37] using male Sprague–Dawley rats (250 to 320 g, N = 5) under urethane anesthesia (1.5 mg/kg, intraparotenial). For the IV dose–response effects of **8a**, control waveform averages were first computed using 60 consecutive paired-stimuli over a 10 min period. MK-801 (0.05 mg/kg, IV; Tocris Bioscience, Bristol, U.K.) was then administered, and after a 5-min waiting period, paired-pulse averaging was again conducted over the next two consecutive 5-min time bins. The total MK-801 response was then computed by combining these two averages. At the end of the second 5-min data collection time bin (i.e., 15 min after MK-801 injection), cumulative IV administration of **8a** (0.001 and 0.03 mg/kg) was initiated. Similar to how the data were handled following MK-801 dosing, 5 min were allowed between each successive **8a** injection and the start of the subsequent averaging. If no effect was observed before the end of the second 5-min averaging period then the two 5-min averages were combined as a single value for that dose and the next IV dose was given. If an effect was observed at any point during the first two averages following a given dose, then two additional 5-min averages were combined as the data point for that dose. The reversal of the MK-801 effects by **8a** did not occur in a typical cumulative dose–response manner, but rather as an all-or-none effect with variable threshold doses between animals. Since reversal was an all-or-none effect once the threshold dose in a particular animal was reached, no additional cumulative doses of **8a** were given. Instead, responses to the paired-pulse stimulations were recorded continuously and averaged over each consecutive 10-min time-bin following a specific dose of **8a**. Mean effects in the **8a** doses were compared to both the control (vehicle) and MK-801 doses using a two-tailed Student's t test (Microsoft Excel, Microsoft Corporation, Redmond, WA). A value of $p < 0.05$ indicated a statistically significant effect.

■ ASSOCIATED CONTENT

Ⓢ Supporting Information

Experimental procedures and characterization data for formation of **18**–**21**. This material is available free of charge via the Internet at http://pubs.acs.org.

Accession Codes

Coordinates and structure factors have been deposited with the Protein Data Bank for complexes of compounds **4** (4LZ5), **7** (4LZ7), and **11** (4LZ8).

■ AUTHOR INFORMATION

Corresponding Authors

*(C.J.O.) Tel: (860) 715-4118. E-mail: christopher.j.odonnell@pfizer.com.

*(J.P.) Tel: (860) 441-3738. E-mail: jayvardhan.pandit@pfizer.com.

Present Addresses

†(N.C.P., X.J.H., A.N.H., C.L.S.) Pfizer Worldwide Research and Development, 700 Main Street, Cambridge, Massachusetts 02139, United States.

‡(J.S.) Genentech, Inc., South San Francisco, California 94080, United States.

§(D.K.B.) Bristol-Myers Squibb Company, Wallingford, Connecticut 06492, United States.

∥(D.M.) Vanderbilt Center for Neuroscience Drug Discovery, Vanderbilt University Medical Center, Nashville, Tennessee 37232, United States.

⊥(M.H.) Yale School of Medicine, New Haven, Connecticut 06510, United States.

#(R.S.H.) Amgen, Inc., Cambridge, Massachusetts 02139, United States.

Notes

The authors declare no competing financial interest.

■ ACKNOWLEDGMENTS

We thank Dr. Jon Bordner and Dr. Brian Samas for the single-crystal X-ray structure of **8a** and Dr. Klaas Schildknegt for his radiosynthetic expertise. We also thank the Pfizer World Wide Medicinal Chemistry Analytical Group for setting up the MS and NMR assays for structure determination and Daniel Virtue and Robert Depianta for chiral separations. We are also grateful to Dr. Russell Dushin and Dr. Katherine Brighty for their review and helpful suggestions in preparing this manuscript.

■ ABBREVIATIONS USED

DHI, dihydroisoxazole; mES, mouse embryonic stem; ATD, amino-terminal domain; FLIPR, fluorometric imaging plate reader; TPSA, topological polar surface area; MDCK, Madin Darby Canine Kidney; CL_H, hepatic clearance; $P_{app,A\rightarrow B}$, absorptive apparent permeabilities; $P_{app,B\rightarrow A}$, secretory apparent permeabilities; $C_{b,u}$, unbound brain compound concentration; $C_{p,u}$, unbound plasma compound concentration; C_{ISF}, interstitial fluid drug concentration; TI, therapeutic index; BCRP, breast cancer resistance protein; PPF, paired-pulse facilitation; Pyr, pyrrolidine

■ REFERENCES

(1) Parsons, C. G.; Danysz, W.; Zieglgaensberger, W. Excitatory amino acid neurotransmission. *Handb. Exp. Pharmacol.* **2005**, *169*, 249−303 Anxiety and Anxiolytic Drugs.

(2) Lynch, G. Memory enhancement: the search for mechanism-based drugs. *Nat. Neurosci.* **2002**, *5* (Suppl), 1035−1038.

(3) (a) Malinow, R.; Malenka, R. C. AMPA receptor trafficking and synaptic plasticity. *Annu. Rev. Neurosci.* **2002**, *25*, 103−126. (b) Lynch, G.; Gall, C. M. Ampakines and the threefold path to cognitive enhancement. *Trends Neurosci.* **2006**, *29*, 554−562.

(4) Morris, R. G. M. Long-term potentiation and memory. *Philos. Trans. R. Soc. London B* **2003**, *358*, 643−647.

(5) (a) Kinney, G. G.; Patino, P.; Mermet-Bouvier, Y.; Starrett, J. E., Jr.; Gribkoff, V. K. Cognition-enhancing drugs increase stimulated hippocampal θ rhythm amplitude in the urethane-anesthetized rat. *J. Pharmacol. Exp. Ther.* **1999**, *291*, 99−106. (b) Hampson, R. E.; Espana, R. A.; Rogers, G. A.; Porrino, L. J.; Deadwyler, S. A. Mechanisms underlying cognitive enhancement and reversal of cognitive deficits in nonhuman primates by the ampakine CX717. *Psychopharmacology* **2009**, *202*, 355−369.

(6) (a) Roberts, B. M.; Holden, D. E.; Shaffer, C. L.; Seymour, P. A.; Menniti, F. S.; Schmidt, C. J.; Williams, G. V.; Castner, S. A. Prevention of ketamine-induced working memory impairments by AMPA potentiators in a nonhuman primate model of cognitive dysfunction. *Behav. Brain Res.* **2010**, *212*, 41−48. (b) Black, M. D. Therapeutic potential of positive AMPA modulators and their relationship to AMPA receptor subunits. A review of preclinical data. *Psychopharmacology* **2005**, *179*, 154−163.

(7) Marenco, S.; Weinberger, D. R. Therapeutic potential of positive AMPA receptor modulators in the treatment of neuropsychiatric disorders. *CNS Drugs* **2006**, *20*, 173−185.

(8) (a) O'Neill, M. J.; Bleakman, D.; Zimmerman, D. M.; Nisenbaum, E. S. AMPA receptor potentiators for the treatment of CNS disorders. *Curr. Drug Targets: CNS Neurol. Disord.* **2004**, *3*, 181−194. (b) Gainetdinov, R. R.; Mohn, A. R.; Bohn, L. M.; Caron, M. G. Glutamatergic modulation of hyperactivity in mice lacking the dopamine transporter. *Proc. Natl. Acad. Sci. U.S.A.* **2001**, *98*, 11047−11054.

(9) (a) Traynelis, S. F.; Wollmuth, L. P.; McBain, C. J.; Menniti, F. S.; Vance, K. M.; Ogden, K. K.; Hansen, K. B.; Yuan, H.; Myers, S. J.; Dingledine, R. Glutamate receptor ion channels: structure, regulation, and function. *Pharmacol. Rev.* **2010**, *62*, 405−496. (b) Wisden, W.; Seeburg, P. H. Mammalian ionotropic glutamate receptors. *Curr. Opin. Neurobiol.* **1993**, *3*, 291−298.

(10) Monyer, H.; Seeburg, P. H.; Wisden, W. Glutamate-operated channels: developmentally early and mature forms arise by alternative splicing. *Neuron* **1991**, *6*, 799−810.

(11) Pei, W.; Huang, Z.; Wang, C.; Han, Y.; Park, J. S.; Niu, L. Flip and Flop: A Molecular Determinant for AMPA Receptor Channel Opening. *Biochemistry* **2009**, *48*, 3767−3777.

(12) Hansen, K. B.; Yuan, H.; Traynelis, S. F. Structural aspects of AMPA receptor activation, desensitization and deactivation. *Curr. Opin. Neurobiol.* **2007**, *17*, 281−288.

(13) (a) Mayer, M. L. Glutamate receptors at atomic resolution. *Nature* **2006**, *440*, 456−462. (b) Jin, R.; Banke, T. G.; Mayer, M. L.; Traynelis, S. F.; Gouaux, E. Structural basis for partial agonist action at ionotropic glutamate receptors. *Nat. Neurosci.* **2003**, *6*, 803−810.

(14) Partin, K. M.; Fleck, M. W.; Mayer, M. L. AMPA receptor flip/flop mutants affecting deactivation, desensitization, and modulation by cyclothiazide, aniracetam, and thiocyanate. *J. Neurosci.* **1996**, *16*, 6634−6647.

(15) Grove, S. J. A.; Jamieson, C.; Maclean, J. K. F.; Morrow, J. A.; Rankovic, Z. Positive allosteric modulators of the α-amino-3-hydroxy-5-methyl-4-isoxazolepropionic acid (AMPA) receptor. *J. Med. Chem.* **2010**, *53*, 7271−7279.

(16) (a) Lynch, G.; Kessler, M.; Rogers, G.; Ambros-Ingerson, J.; Granger, R.; Schehr, R. S. Psychological effects of a drug that facilitates brain AMPA receptors. *Int. Clin. Psychopharmacol.* **1996**, *11*, 13−19. (b) Granger, R.; Staubli, U.; Davis, M.; Perez, Y.; Nilsson, L.; Rogers, G. A.; Lynch, G. A drug that facilitates glutamatergic transmission reduces exploratory activity and improves performance in a learning-dependent task. *Synapse* **1993**, *15*, 326−329.

(17) Rosi, S.; Grazia Giovannini, M.; Lestage, P. J.; Munoz, C.; Della Corte, L.; Pepeu, G. S18986, a positive modulator of AMPA receptors with cognition-enhancing properties, increases ACh release in the hippocampus of young and aged rat. *Neurosci. Lett.* **2004**, *361*, 120−123.

(18) Ward, S. E.; Harries, M.; Aldegheri, L.; Austin, N. E.; Ballantine, S.; Ballini, E.; Bradley, D. M.; Bax, B. D.; Clarke, B. P.; Harris, A. J.; Harrison, S. A.; Melarange, R. A.; Mookherjee, C.; Mosley, J.; Dal Negro, G.; Oliosi, B.; Smith, K. J.; Thewlis, K. M.; Woollard, P. M.; Yusaf, S. P. Integration of lead optimization with crystallography for a membrane-bound ion channel target: discovery of a new class of AMPA receptor positive allosteric modulators. *J. Med. Chem.* **2011**, *54*, 78−94.

(19) Ornstein, P. L.; Zimmerman, D. M.; Arnold, M. B.; Bleisch, T. J.; Cantrell, B.; Simon, R.; Zarrinmayeh, H.; Baker, S. R.; Gates, M.; Tizzano, J. P.; Bleakman, D.; Mandelzys, A.; Jarvie, K. R.; Ho, K.; Deverill, M.; Kamboj, R. K. Biarylpropylsulfonamides as novel, potent potentiators of 2-amino-3-(5-methyl-3-hydroxyisoxazol-4-yl)propanoic acid (AMPA) receptors. *J. Med. Chem.* **2000**, *43* (23), 4354−4358.

(20) Zarrinmayeh, H.; Tromiczak, E.; Zimmerman, D. M.; Rankl, N.; Ho, K. H.; Dominguez, E.; Castano, A.; Escribano, A.; Fernandez, C.; Jimenez, A.; Hornback, W. J.; Nisenbaum, E. S. A novel class of positive allosteric modulators of AMPA receptors: design, synthesis, and structure−activity relationships of 3-biphenyl-4-yl-4-cyano-5-ethyl-1-methyl-1*H*-pyrrole-2-carboxylic acid, LY2059346. *Bioorg. Med. Chem. Lett.* **2006**, *16*, 5203−5206.

(21) Ward, S. E.; Harries, M.; Aldegheri, L.; Andreotti, D.; Ballantine, S.; Bax, B. D.; Harris, A. J.; Harker, A. J.; Lund, J.; Melarange, R.; Mingardi, A.; Mookherjee, C.; Mosley, J.; Neve, M.; Oliosi, B.; Profeta, R.; Smith, K. J.; Smith, P. W.; Spada, S.; Thewlis, K. M.; Yusaf, S. P. Discovery of *N*-[(2*S*)-5-(6-fluoro-3-pyridinyl)-2,3-dihydro-1*H*-inden-2-yl]-2-propanesulfonamide, a novel clinical AMPA receptor positive modulator. *J. Med. Chem.* **2010**, *53*, 5801−5812.

(22) Zarrinmayeh, H.; Bleakman, D.; Gates, M. R.; Yu, H.; Zimmerman, D. M.; Ornstein, P. L.; McKennon, T.; Arnold, M. B.; Wheeler, W. J.; Skolnick, P. [3*H*]*N*-2-(4-(*N*-benzamido)phenyl)-propyl-2- propanesulfonamide: a novel AMPA receptor potentiator and radioligand. *J. Med. Chem.* **2001**, *44*, 302−304.

(23) McNeish, J.; Roach, M.; Hambor, J.; Mather, R. J.; Weibley, L.; Lazzaro, J.; Gazard, J.; Schwarz, J.; Volkmann, R.; Machacek, D.; Stice, S.; Zawadzke, L.; O'Donnell, C.; Hurst, R. High-throughput screening

in embryonic stem cell-derived neurons identifies potentiators of α-amino-3-hydroxyl-5-methyl-4-isoxazolepropionate-type glutamate receptors. *J. Biol. Chem.* **2010**, *285*, 17209−17217.
(24) (a) Barbachyn, M. R.; Ford, C. W. Oxazolidinone structure−activity relationships leading to linezolid. *Angew. Chem., Int. Ed.* **2003**, *42*, 2010−2023. (b) Barbachyn, M. R.; Cleek, G. J.; Dolak, L. A.; Garmon, S. A.; Morris, J.; Seest, E. P.; Thomas, R. C.; Toops, D. S.; Watt, W.; Wishka, D. G.; Ford, C. W.; Zurenko, G. E.; Hamel, J. C.; Schaadt, R. D.; Stapert, D.; Yagi, B. H.; Adams, W. J.; Friis, J. M.; Slatter, J. G.; Sams, J. P.; Oien, N. L.; Zaya, M. J.; Wienkers, L. C.; Wynalda, M. A. Identification of phenylisoxazolines as novel and viable antibacterial agents active against Gram-positive pathogens. *J. Med. Chem.* **2003**, *46*, 284−302.
(25) (a) Wager, T. T.; Hou, X.; Verhoest, P. R.; Villalobos, A. Moving beyond rules: the development of a central nervous system multiparameter optimization (CNS MPO) approach to enable alignment of druglike properties. *ACS Chem. Neurosci.* **2010**, *1*, 435−449. (b) Lipinski, C. A. Lead- and drug-like compounds: the rule-of-five revolution. *Drug Discovery Today: Technol.* **2004**, *1*, 337−341.
(26) Hop, C. E. C. A.; Cole, M. J.; Davidson, R. E.; Duignan, D. B.; Federico, J.; Janiszewski, J. S.; Jenkins, K.; Krueger, S.; Lebowitz, R.; Liston, T. E.; Mitchell, W.; Snyder, M.; Steyn, S. J.; Soglia, J. R.; Taylor, C.; Troutman, M. D.; Umland, J.; West, M.; Whalen, K. M.; Zelesky, V.; Zhao, S. X. High throughput ADME screening: practical considerations, impact on the portfolio and enabler of in silico ADME models. *Curr. Drug Metab.* **2008**, *9*, 847−853.
(27) (a) Timm, D. E.; Benveniste, M.; Weeks, A. M.; Nisenbaum, E. S.; Partin, K. M. Structural and functional analysis of two new positive allosteric modulators of GluA2 desensitization and deactivation. *Mol. Pharmacol.* **2011**, *80*, 267−280. (b) Sun, Y.; Olson, R.; Horning, M.; Armstrong, N.; Mayer, M.; Gouaux, E. Mechanism of glutamate receptor desensitization. *Nature* **2002**, *417*, 245−253. (c) Jin, R.; Clark, S.; Weeks, A. M.; Dudman, J. T.; Gouaux, E.; Partin, K. M. Mechanism of positive allosteric modulators acting on AMPA receptors. *J. Neurosci.* **2005**, *25*, 9027−9036. (d) Ahmed, A. H.; Ptak, C. P.; Oswald, R. E. Molecular mechanism of flop selectivity and subsite recognition for an AMPA receptor allosteric modulator: structures of GluA2 and GluA3 in complexes with PEPA. *Biochemistry* **2010**, *49*, 2843−2850.
(28) (a) Marrone, T. J.; Luty, B. A.; Rose, P. W. Discovering high-affinity ligands from the computationally predicted structures and affinities of small molecules bound to a target: a virtual screening approach. *Perspect. Drug Discovery Des.* **2000**, *20*, 209−230. (b) Gehlhaar, D. K.; Verkhivker, G. M.; Rejto, P. A.; Sherman, C. J.; Fogel, D. B.; Fogel, L. J.; Freer, S. T. Molecular recognition of the inhibitor AG-1343 by HIV-1 protease: conformationally flexible docking by evolutionary programming. *Chem. Biol.* **1995**, *2*, 317−324.
(29) Linden, A. M.; Yu, H.; Zarrinmayeh, H.; Wheeler, W. J.; Skolnick, P. Binding of an AMPA receptor potentiator ([3H]-LY395153) to native and recombinant AMPA receptors. *Neuropharmacology* **2001**, *40*, 1010−1018.
(30) (a) Stepan, A. F.; Walker, D. P.; Bauman, J.; Price, D. A.; Baillie, T. A.; Kalgutkar, A. S.; Aleo, M. D. Structural alert/reactive metabolite concept as applied in medicinal chemistry to mitigate the risk of idiosyncratic drug toxicity: a perspective based on the critical examination of trends in the top 200 drugs marketed in the United States. *Chem. Res. Toxicol.* **2011**, *24*, 1345−1410. (b) Kalgutkar, A. S.; Gardner, I.; Obach, R. S.; Shaffer, C. L.; Callegari, E.; Henne, K. R.; Mutlib, A. E.; Dalvie, D. K.; Lee, J. S.; Nakai, Y.; O'Donnell, J. P.; Boer, J.; Harriman, S. P. A comprehensive listing of bioactivation pathways of organic functional groups. *Curr. Drug Metab.* **2005**, *6*, 161−225.
(31) Tillement, J. P.; Urien, S.; Chaumet-Riffaud, P.; Riant, P.; Bree, F.; Morin, D.; Albengres, E.; Barre, J. Blood binding and tissue uptake of drugs. Recent advances and perspectives. *Fundam. Clin. Pharmacol.* **1988**, *2*, 223−238.
(32) Shaffer, C. L. Defining neuropharmacokinetic parameters in CNS drug discovery to determine cross-species pharmacologic exposure-response relationships. *Annu. Rep. Med. Chem.* **2010**, *45*, 55−70.
(33) (a) Liu, X.; Van Natta, K.; Yeo, H.; Vilenski, O.; Weller, P. E.; Worboys, P. D.; Monshouwer, M. Unbound drug concentration in brain homogenate and cerebral spinal fluid at steady state as a surrogate for unbound concentration in brain interstitial fluid. *Drug Metab. Dispos.* **2009**, *37*, 787−793. (b) Doran, A. C.; Osgood, S. M.; Mancuso, J. Y.; Shaffer, C. L. An evaluation of using rat-derived single-dose neuropharmacokinetic parameters to project accurately large animal unbound brain drug concentrations. *Drug Metab. Dispos.* **2012**, *40*, 2162−2173.
(34) (a) Yamada, K. A. Modulating excitatory synaptic neurotransmission: potential treatment for neurological disease? *Neurobiol. Dis.* **1998**, *5*, 67−80. (b) Garthwaite, G. G. Mechanisms of AMPA neurotoxicity in rat brain slices. *Eur. J. Neurosci.* **1991**, *3*, 729−736. (c) Di, L.; Umland, J. P.; Chang, G.; Huang, Y.; Lin, Z.; Scott, D. O.; Troutman, M. D.; Liston, T. E. Species independence in brain tissue binding using brain homogenates. *Drug Metab. Dispos.* **2011**, *39*, 1270−1277.
(35) Shaffer, C. L.; Hurst, R. S.; Scialis, R. J.; Osgood, S. M.; Bryce, D. K.; Hoffmann, W. E.; Lazzaro, J. T.; Hanks, A. N.; Lotarski, S.; Weber, M. L.; Liu, J.; Menniti, F. S.; Schmidt, C. J.; Hajós, M. Positive allosteric modulation of AMPA receptors from efficacy to toxicity: the interspecies exposure-response continuum of the novel potentiator PF-4778574. *J. Pharmacol. Exp. Ther.* **2013**, *347*, 212−224.
(36) Ryder, J. W.; Falcone, J. F.; Manro, J. R.; Svensson, K. A.; Merchant, K. M. Pharmacological characterization of cGMP regulation by the biarylpropylsulfonamide class of positive, allosteric modulators of α-amino-3-hydroxy-5-methyl-4-isoxazolepropionic acid receptors. *J. Pharmacol. Exp. Ther.* **2006**, *319*, 293−298.
(37) Kiss, T.; Hoffmann, W. E.; Hajos, M. Delta oscillation and short-term plasticity in the rat medial prefrontal cortex: modelling NMDA hypofunction of schizophrenia. *Int. J. Neuropsychopharmacol.* **2011**, *14*, 29−42.
(38) Olney, J. W.; Newcomer, J. W.; Farber, N. B. NMDA receptor hypofunction model of schizophrenia. *J. Psychiatr. Res.* **1999**, *33*, 523−533.
(39) Goldman-Rakic, P. S. Working memory dysfunction in schizophrenia. *J. Neuropsychiatry Clin. Neurosci.* **1994**, *6*, 348−357.
(40) Moghaddam, B.; Javitt, D. From revolution to evolution: the glutamate hypothesis of schizophrenia and its implication for treatment. *Neuropsychopharmacology* **2012**, *37*, 4−15.
(41) Shaffer, C. L.; Scialis, R. J.; Rong, H.; Obach, R. S. Using Simcyp to project human oral pharmacokinetic variability in early drug research to mitigate mechanism-based adverse events projecting human C_{max} variability after an oral dose via PBPK modeling. *Biopharm. Drug Dispos.* **2012**, *33*, 72−84.